POLITECNICO DI TORINO
Repository ISTITUZIONALE

Convective-absolute nature of ripple instabilities on ice and icicles

Terms of use:

Publisher copyright

(Article begins on next page)

05 May 2024

Convective-absolute nature of ripple instabilities on ice and icicles

Carlo Camporeale,[*] Riccardo Vesipa,[†] and Luca Ridolfi[‡]

Politecnico di Torino, DIATI, Corso Duca degli Abruzzi 24, Torino, Italy

(Received 13 May 2016; published 25 May 2017)

Film hydrodynamics is crucial in water-driven morphological pattern formation. A prominent example is given by icicle ripples and ice ripples, which are regular patterns developing on freezing-melting inclined surfaces bounding open-channel flows. By a suitable mathematical model based on conservation principles and the use of the cusp map method, in this paper we address the convective-absolute nature of these two kinds of instabilities. The obtained results show that icicle ripples, which develop at inverted (overhang) conditions, have subcentimetric wavelengths which are unstable when the Reynolds number of the liquid flow (Re) is small and the supercooling is intensive. With the increase in Re, the instability switches from absolute to convective. Ice ripples instead exhibit the opposite dependance on Re and are highly affected by the surface slope. In addition, the evaluation of the so-called absolute wave number, which is responsible for the asymptotic impulse response, suggests a different interpretation of some recent experiments about ice ripples.

I. INTRODUCTION

Regular patterns which develop on deformable interfaces between solid matter and a flowing fluid are ubiquitous in geophysics. Formidable examples are desert dunes [1], snow megadunes [2], river bed forms [3], carbonatic patterns in karst caves [4], and melting-freezing instabilities [5], such as ice and icicle ripples. This work deals with the last category, where mutual interactions between an iced flat incline and a laminar water film are involved in a so-called open-boundary Stefan-like problem [6].

Basically, ice ripples develop on gently inclined surfaces at relatively high Reynolds numbers [see Fig. 1(a)], whereas icicle ripples require lower flow rates, subvertical conditions, and supercooled dripping water (namely, slightly under 0 °C). The existing mathematical attempts to model icicle ripples perform perturbations of a planar incline in a Cartesian approximation, thus neglecting the cylindrical geometry. Henceforth, when referring to the icicle regime, we therefore assume the same approximation. Although icicle and ice ripples evolve under different conditions and exhibit different features they can be tackled using a similar mathematical modeling.

Film hydrodynamics plays a key role in triggering and ruling all the above-mentioned examples of pattern formation. Therefore, strong similarities exist among the morphological instabilities that develop in different environments. For example, the karst counterpart of an icicle ripple is called a crenulation, which develops on the surface of karst stalactites [8], whereas ice ripples are akin to river antidunes, as recently pointed out in Ref. [9].

Since the early investigations made in this field—such as the ripple formation on the underside of river ice covers [10], the analysis of antidune patterns inside freezing pipes [11], or the analytical treatments of icicle [12,13] and ice ripples [14]—it has been evident that the understanding of fluid-dynamic-related mechanisms is of paramount importance. In fact, the phenomena herein investigated are strictly related to the linearized equations of mass, momentum, and heat conservation for the liquid. Recent experiments have also emphasized the key role of impurities in water in triggering

---

[*]carlo.camporeale@polito.it

[†]riccardo.vesipa@polito.it
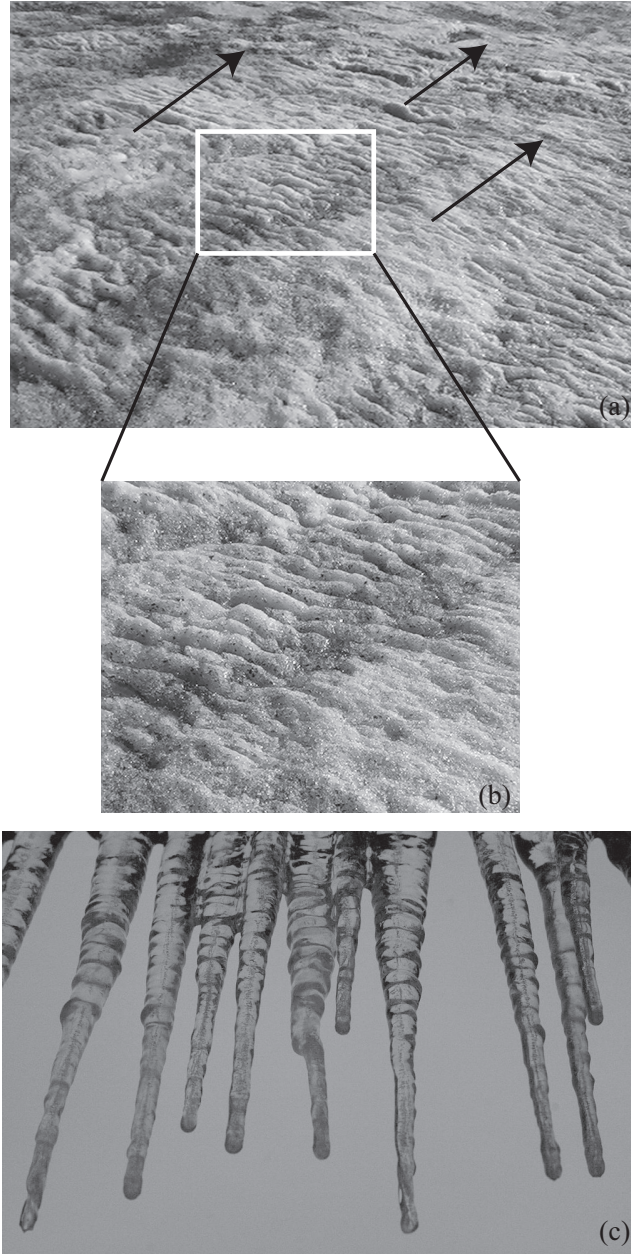
[‡]luca.ridolfi@polito.it

FIG. 1. (a) An example of ice ripples observed on the upper surface of the Ciardoney glacier (northern Italy, 45°31′ N, 7°23′ E; altitude 3100 m). The arrows indicate the slope of the bed and the direction of the melting flow. (b) Closeup of (a). The longitudinal wavelength is about 0.1 m. Other data and pictures can be found in Ref. [7]. (c) Example of icicles with ripplelike protuberances (courtesy of Wingchi Poon). In (c), the dripping water likely contains impurities.

centimetric wavelength, but the underlaying mechanisms have not been delineated yet [15]. We neglect the role of salt impurities in the water and address an Orr-Sommerfeld problem involving free surface boundary conditions and the thermodynamics of the liquid-solid interface (namely, the Stefan condition). Under this perspective, the topic is close to some classical problems in

hydrodynamic stability theory involving free shear flows, with the novelty that the liquid-solid interface evolves dynamically. It is then expected that many refined techniques, adopted in standard hydrodynamic theory, can therefore be extended to these kinds of morphological instabilities in order to tackle some important open issues.

For instance, previous works have shown the mechanism of instability through a formal linear stability analysis, but the question of whether the instability is convective or absolute remains unexplored. This is the main goal of the present work. By definition, a system is convectively unstable if the response to an impulsive perturbation increases in time but migrates and decays to zero at all the spatial locations, and it is absolutely unstable if the response grows exponentially in time at all spatial locations [16]. Convectively unstable systems behave as "noise amplifiers," displaying extrinsic dynamics, since in the absence of continuous forcing the response decays back to zero, whereas absolutely unstable systems are characterized by intrinsic dynamics and behave as "oscillators" [17].

The knowledge of the type of instability is fundamental for correctly understanding field observations and for an appropriate setup of numerical simulations and experiments. We show that the characterization of the convective-absolute nature of the instability can provide a different interpretation of the results obtained by the laboratory experiments reported in Ref. [15]. Furthermore, the evaluation of the absolute wave number (see later) will be functional to a new view of the experiments made in Ref. [9] where ice ripples were reproduced for the first time.

Addressing the nature of the instability is not a trivial task when the dispersion relation is not analytically known, and this is the case for freezing-melting problems coupled with film hydrodynamics. For this reason, we adopt the cusp map method which only requires the eigenvalue problem to be solved for a set of complex wave numbers [16]. The same method has been successful in addressing the convective-absolute nature of alluvial dunes and antidunes (see [18]).

II. MATHEMATICAL DEVELOPMENTS

A. Governing equations

From a mathematical viewpoint, we are going to address a Stefan-type problem, where a thin film with a free surface thermally interacts with a freezing-melting interface. The complete set of governing equations has been already formulated and discussed in different previous works [9,13,14,19]. In the following we adopt the same formalism and notation of [14], which the reader can refer to for a thorough justification of the equations. The only novelty is in the icicle case, where the water film is considered supercooled and, then, a new boundary condition is required. Henceforth, we distinguish the *planar* case (ice ripples) and the *icicle* case frameworks by referring to cases P and I, respectively.

Let us consider a free-surface viscous liquid flowing over a phase-change interface that, at the base state, is flat and inclined at the angle β (see Fig. 2). The variables are made dimensionless using the Nusselt solution for the free surface velocity, $\tilde{U}_F = (9g \sin \beta q^2/8\nu)^{1/3}$, the stream depth, $\tilde{D}_0 = (3\nu q/g \sin \beta)^{1/3}$, and the morphological time scale of the interface evolution, $\tau = \tilde{D}_0^2/\gamma_s \mathrm{St}$, where ν is the kinematic viscosity, g is gravity acceleration, q is the flow rate per unit width, γ_s is the thermal solid diffusivity, $\mathrm{St} = c_s \Delta/\lambda$ is the Stefan number, c_s is the ice heat capacity, and λ is the latent heat. The Reynolds number, $\mathrm{Re} = \tilde{U}_F \tilde{D}_0/\nu$, is regarded as a parameter. Temperatures are made dimensionless with the difference Δ between the temperature of the liquid-solid interface and the temperature taken inside the ice at a distance $\tilde{S}_0$ from the interface. Although the latter difference is usually unknown, reference values could be taken around $1°C$. However, it should be noticed that the dimensionalization of equations allows one to address the following stability analysis without setting a specific value of Δ. In the planar case (P), $\tilde{S}_0$ is of the order of the thermal boundary layer inside the ice, whereas in the icicle case (I), $\tilde{S}_0$ is the radius of the icicle.

The main physical assumptions are (i) a laminar regime, (ii) no buoyancy effects, (iii) the fluid-dynamic response of the gas phase over the liquid free surface is neglected, and (iv) the morphological
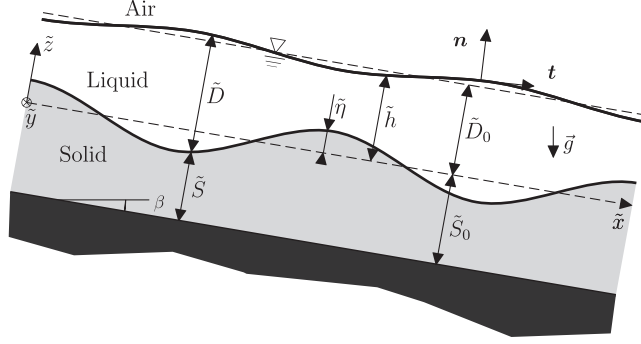
FIG. 2. Sketch of the physical problem. Dashed line, unperturbed, flat interface; continuous line, perturbed interface. The black region is the undisturbed region.

time scale $\tilde{\tau}$ is much larger than the hydrodynamic time scale $\tilde{D}_0^2/\nu\mathrm{Re}$. Finally, for case P only, an additional hypothesis is that the liquid-solid interface is at dynamical thermal equilibrium. This last hypothesis has been recently questioned [9] because it precluded their experimental observations to be compared with the theory of ice ripples. Therefore, it was substituted [9] by a "frozen time approximation" in which the interface at the base state is considered time dependent [e.g., 20,21], but the time variation is so slow it can be assumed to be negligible. From the results reported in Ref. [9], it is evident that both approaches provided very similar results. In case I, we instead assume the frozen time approximation, since the rate of the icicle's growth is an important factor of the model.

Under the above conditions, the mathematical problem is composed by the following versions of the continuity equation, Navier-Stokes equations, and heat conservation equation for the liquid and solid phase:

$$\boldsymbol{\nabla} \cdot \mathbf{u} = 0, \tag{1}$$

$$\mathbf{u} \cdot \boldsymbol{\nabla}\mathbf{u} = \mathrm{Re}^{-1}\nabla^2\mathbf{u} - \boldsymbol{\nabla}p + \boldsymbol{\delta}, \quad z \in [\eta, \eta + D], \tag{2}$$

$$\mathbf{u} \cdot \boldsymbol{\nabla}\Theta = \mathrm{Pe}^{-1}\nabla^2\Theta, \quad z \in [\eta, \eta + D], \tag{3}$$

$$\nabla^2\Theta = 0, \quad z \in [-S, \eta], \tag{4}$$

where $\boldsymbol{\delta} = g\tilde{D}_0\tilde{U}_f^{-2}(\sin\beta, 0, -\cos\beta)$, $\mathbf{u} = \{u, v, w\}$ is the flow field vector in the film, Pe is the Peclet number, and Θ is temperature. The boundary conditions are

$$(z = \eta) \begin{cases} \mathbf{t} \cdot \mathbf{u} = 0, \tag{5a} \\[2mm] \left[u\frac{\partial}{\partial x} + v\frac{\partial}{\partial y}\right]\eta = w, \tag{5b} \\[2mm] \left[\frac{\partial\Theta}{\partial z} - \frac{\partial\Theta}{\partial x}\frac{\partial\eta}{\partial x} - \frac{\partial\Theta}{\partial y}\frac{\partial\eta}{\partial y}\right]_{\eta^-} - r_k\left[\frac{\partial\Theta}{\partial z} - \frac{\partial\Theta}{\partial x}\frac{\partial\eta}{\partial x} - \frac{\partial\Theta}{\partial y}\frac{\partial\eta}{\partial y}\right]_{\eta^+} = \frac{\partial\eta}{\partial t}, \tag{5c} \end{cases}$$

$$(z = \eta + D) \begin{cases} \left[u\frac{\partial}{\partial x} + v\frac{\partial}{\partial y}\right](\eta + D) = w, \tag{6a} \\[2mm] \mathbf{n} \cdot \mathbf{T} \cdot \mathbf{n} + \frac{\mathrm{Re}}{\mathrm{We}^2}\mathcal{K} = \mathbf{n} \cdot \mathbf{T} \cdot \mathbf{t} = 0, \tag{6b} \end{cases}$$

$$\text{(case P)} \begin{cases} \mathbf{n} \cdot \mathbf{\nabla}\Theta = (r_\kappa S_0)^{-1} & (z = \eta + D) & \text{(7a)} \\ \frac{\partial \Theta}{\partial z} = S_0^{-1} & (z = -S) & \text{(7b)} \\ \Theta = 0 & (z = \eta), & \text{(7c)} \end{cases}$$

$$\text{(case I)} \begin{cases} \Theta = \Theta_0^F & (z = \eta + D) & \text{(8a)} \\ \left\langle \frac{\partial \Theta}{\partial z}\big|_{\eta^-} \right\rangle = f(V) & (z = \eta) & \text{(8b)} \\ \Theta = 0 & (z = \eta), & \text{(8c)} \end{cases}$$

where $\mathbf{n}$ and $\mathbf{t}$ are the unit normal and tangent vector to a generic surface, respectively, $\mathbf{T} = p\,\mathrm{Re}\,\mathbf{I} - 2\mathbf{D}$ is the dimensionless Newtonian stress tensor (with $\mathbf{I}$ and $\mathbf{D}$ the identity matrix and the rate-of-strain tensor, respectively), $\mathcal{K}$ is the local mean curvature of the free surface, We $= \tilde{U}_F(\rho \tilde{D}_0/\sigma)^{1/2}$ is the Weber number (where ρ and σ are the density and the surface tension of the liquid, respectively), r_κ is the ratio of the liquid to solid thermal conductivity, and V is the rate of icicle growth. Equations (5a)–(5c) state, respectively, no-slip and melting conditions, impermeability of the interface, and the Stefan condition (i.e., heat conservation at the interface). Equations (6a) and (6b) state, respectively, kinematic and dynamic conditions at the free surface.

The thermal boundary conditions are set in a different way between the two configurations. For the planar case, the hypothesis of the dynamic thermal equilibrium allows the heat flux at the free surface to be equal to the one at the internal edge of the thermal boundary layer in the ice [Eqs. (7a) and (7b)]. On the contrary, the icicle configuration is much more involved, since it suffers from two uncertainties. First, due to the supercooling of the dripping film, there is no dynamic thermal equilibrium at all, but an overall icicle growth rate, V, is present. This places the system far from equilibrium. The exact approach should go through the modeling of the air boundary layer, thus enabling a heat flux condition at the free surface (which involves Dirichlet terms as well, namely, a Robin condition). With the aim of maintaining the model as simply as possible, we opted for neglecting the air thermofluid dynamics, and we set a Dirichlet condition at the free surface [Eq. (8a)]. In this way, as discussed in the last section, the value of the water temperature at the free surface can be related to the room temperature of the air. A second issue is given by the lack of data on the temperature distribution in the interior of the icicle. One could argue that, since there is no source or sink inside, the only possible solution is that the ice is at the melting temperature everywhere. This choice corresponds to a vanishing gradient at the interface. However, because of the icicle tridimensional structure, it is more likely that the icicle is crossed longitudinally by a heat flux, thus making possible the existence of a thermal gradient in the interior-exterior direction as well. We do not know *a priori* this latter heat flux but, through the Stefan equation, the spatially averaged temperature gradient in the ice at the liquid-solid interface must be related to the rate of advancement or retreat of the liquid-solid interface, that is, V [see Eq. (8b), where brackets refer to surface averaging]. The unknown function $f(V)$ is derived in the following on the basis of heat conservation at the interface [see Eqs. (10)–(12)]. Notice that the spatial averaging in this last condition affects the basic state only. Perturbations are not affected since they are in normal mode form and have, therefore, zero average. We show that Eq. (8b) is crucial to ensure a physically acceptable behavior of the relation dispersion at high wave numbers, so solving a shortcoming that was present in the literature. Finally, in both configurations (P and I) the obvious melting temperature must be set at the liquid-solid interface [Eqs. (7c) and (8c)].

B. Linear stability analysis

In order to address the convective-absolute nature of the present problem, it is necessary to linearize Eqs. (1)–(8) around the basic state solution of the Nusselt flow, with flat interface. Although it was shown in Ref. [14] that Squire's theorem does not hold in the present context, because three-dimensional patterns can be more unstable than two-dimensional ones, it suffices here to focus

on transversal perturbations of the basic state, i.e., $\partial_y = v = 0$. The main concern of this work is in fact to investigate the character of ripple instabilities on ice and icicles, which are purely two-dimensional structures.

Furthermore, it is convenient to work in a rectangularized domain that is set through the mapping $z \to \zeta = (z - \eta)/F$, where $F = D(x,t)$ for $\zeta > \eta$ and $F = S(x,t)$ for $\zeta < \eta$.

It is straightforward to show that the basic state solution of the problem (henceforth denoted by subscript zero) is given by

$$u_0 = 2\zeta - \zeta^2, \quad p_0 = \delta_z(\zeta - 1), \quad \theta_0 = \zeta\Theta_0^F, \quad \vartheta_0 = K\zeta, \tag{9}$$

where $\Theta := \theta$ for $\zeta > 0$ and $\Theta := \vartheta$ for $\zeta < 0$, respectively, while $K = 1$ for the P case and $K = f$ for the I case. Furthermore, the Stefan equation written at the basic state reads

$$\frac{1}{S_0}\frac{\partial\vartheta_0}{\partial\zeta} - r_k\frac{\partial\theta_0}{\partial\zeta} = \frac{\partial\eta_0}{\partial t}. \tag{10}$$

The right-hand side of Eq. (10) is zero in the P case, due to the hypothesis of dynamical thermal equilibrium, whereas it is equal to V in the ice case. After substituting Eq. (9) into Eq. (10) we obtain, respectively,

$$S_0 = \left(r_k\Theta_0^F\right)^{-1} \quad \text{(case P)}, \tag{11}$$

$$f = S_0\left(V + r_k\Theta_0^F\right) \quad \text{(case I)}. \tag{12}$$

It should be noticed that the water film is supercooled in icicles (i.e., $\Theta_0^F < 0$) and, in order to ensure negative temperatures even in the ice (corresponding to $f > 0$), Eq. (12) imposes that $V > r_k|\Theta_0^F|$. This condition is indeed confirmed by data reported in previous experiments (e.g., [13,15]). We also observe that if the unperturbed ice growth rate, V, is set to zero then one recovers the hypothesis of the dynamical equilibrium which [through Eq. (11)] imposes $f = 1$, coherently with the solution of ϑ_0 for the planar case.

Taking into account Eq. (1), a normal mode perturbation of the complete problem around Eqs. (9) is

$$\{u,w,p,\theta,\vartheta,\eta,D\} = \{u_0,0,p_0,\theta_0,\vartheta_0,\eta_0(t),1\} + \epsilon\{\phi' + u_0'(1 + d_1\zeta),$$
$$- ik\phi,\theta_1(\zeta),p_1,\vartheta_1(\zeta),1,d_1\}e^{i(kx-\omega t)} + \text{c.c.}, \tag{13}$$

where $\epsilon \ll 1$ is the magnitude of the interface perturbation, $\phi(\zeta)$ is the modified stream function which defines the flow field perturbation, and the apex refers to the ζ derivative.

At the order $O(\epsilon)$, we end up with the linear eigenvalue problem

$$\mathcal{D}^2\phi - \Gamma(u_0\mathcal{D} + 2)\phi = 0, \tag{14}$$

$$(\mathcal{D} - \Gamma u_0)\frac{\theta_1}{\Theta_0^F} + \Lambda\phi + (k - \Lambda u_0)(h_1\zeta + 1) = 0, \tag{15}$$

$$\mathcal{D}_s\vartheta_1 + k^2(1 + \zeta)S_0 = 0, \tag{16}$$

$$\phi'(0) = -2, \quad \phi(0) = \theta_1(0) = \vartheta_1(0) = 0, \tag{17}$$

$$\phi(1) + h_1 = 0, \quad \phi''(1) - h_1(2 + k^2) = 0, \tag{18}$$

$$\phi'''(1) - (3k + \Gamma)\phi'(1) - \Gamma\left(\delta + \frac{k^2}{\text{We}^2}\right)h_1 = 0, \tag{19}$$

$$\theta_1'(1) - d_1\Theta_0^F = 0, \quad \vartheta_1'(-1) - S_0^{-1} = 0 \quad \text{(case P)}, \tag{20}$$
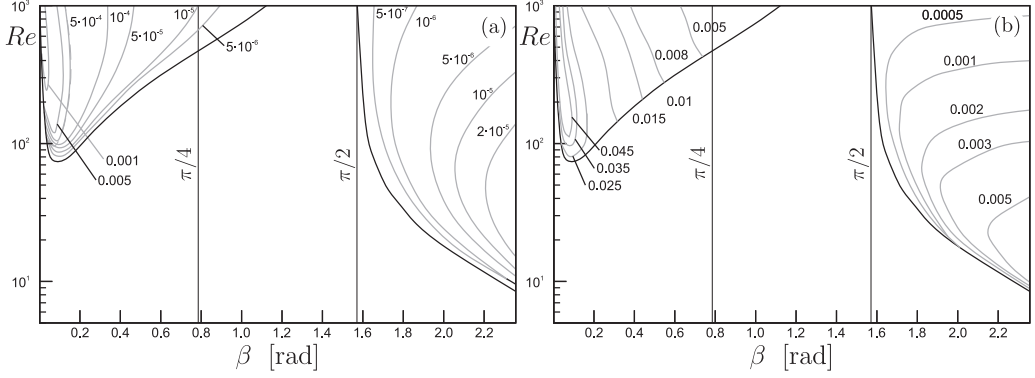
FIG. 3. (a) Growth rate of the perturbation ω_i in the $\{\beta,\mathrm{Re}\}$ plane for $\Theta_0^F = 0.25$. (b) Most linearly unstable wave number k_m. For $0 < \beta < \pi/2$ perturbations always migrate upstream, while for $\beta > \pi/2$ (inverted flow) perturbations always migrate downstream (not reported).

$$\theta_1(1) = 0, \quad \vartheta_1(-1) = 0 \quad \text{(case I)}, \tag{21}$$

$$r_k \theta_1'(0) - \frac{\vartheta_1'(0)}{S_0} - r_k d_1 \Theta_0^F + \frac{1}{S_0^2} = i\omega, \tag{22}$$

where $\mathcal{D} = \partial_{\zeta\zeta} - k^2$, $\mathcal{D}_s = \partial_{\zeta\zeta} - S_0^2 k^2$, $\Gamma = ik\mathrm{Re}$, and $\Lambda = ik\mathrm{Pe}$.

Equation (22) serves as a dispersion relationship which provides the unique eigenvalue ω of the problem by virtue of hypothesis (iv). In case P, the problem in Eqs. (14)–(22) has been solved both numerically, with a spectral Galerkin technique, and semianalytically, through a Frobenius series expansion [14]. The comparison between these two methods has shown that the added discrete set of eigenvalues that would appear if hypothesis (iv) was relaxed has a hydrodynamic nature and does not affect the morphological eigenvalue, namely the one that is here under consideration.

We finally remind that the system is temporally unstable; i.e., it is prone to pattern formation, if $\omega_i \equiv \mathrm{Im}[\omega] > 0$ for some (real) values of the wave number k. The selected wave number k_m is the least stable, that is, $\partial\omega_i/\partial k|_{k=k_m} = 0$, and the corresponding phase celerity is given by $c = \omega_r(k_m)/k_m$.

The main consequence of the different boundary conditions between the icicle (supercooled) case and the planar case is the term $\vartheta_1'(0)$ in the relation dispersion (22), which reads, respectively,

$$\vartheta_1'(0) = \frac{1}{S_0} - k\tanh(kS_0) \quad \text{(case P)}, \tag{23}$$

$$\vartheta_1'(0) = f(V)\left(\frac{1}{S_0} - k\coth(kS_0)\right) \quad \text{(case I)}. \tag{24}$$

Both solutions for this term dampen the high behavior of the relation dispersion at high wave numbers. Since the second term in Eqs. (23) and (24) goes as $\sim -k$ for $k \gg 1$, the factor $f(V)$ is larger, and the damping is more effective. Therefore, the unperturbed ice growth rate V rules the well-posed behavior of the model at high wave numbers. In this way a shortcoming that appeared in some previous models (namely, $\omega_i \to \infty$ for $k \to \infty$) has been resolved (e.g., [13]).

Figure 3 shows typical unstable regions in the parameter plane (β,Re) for the planar case (case P). As also noted in the following, when the film exceeds the vertical condition, $\beta = \pi/2$, the nature of the instability changes. A first symptom of this change is that the least stable perturbations are upstream migrating at $\beta < \pi/2$ and downstream migrating at $\beta > \pi/2$ (not shown in the figure). Indeed, in Fig. 3 two distinct regions of instability appear, pertinent to normal ($\beta < \pi/2$) and inverted ($\beta > \pi/2$) flow, respectively, and are separated by a region of stability. The former region
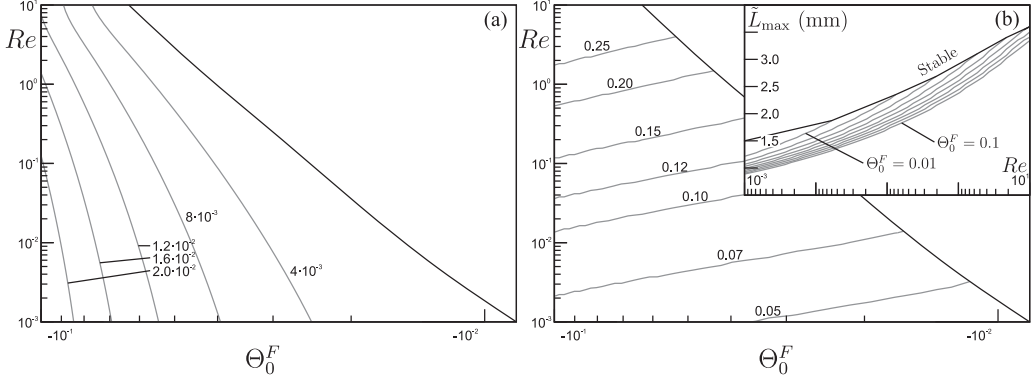
FIG. 4. (a) Growth rate of the perturbation ω_i in the $\{\Theta_0^F, \mathrm{Re}\}$ plane for $\beta = \pi/2$. (b) Most linearly unstable wave number k_m. The inset reports the selected wavelengths in millimeters against the Reynolds number.

corresponds to the domain of existence of ice ripples, which develop at Re of order $O(10^2)$ and small slopes, and which can eventually evolve to cyclic steps [9].

Figure 4 shows the typical unstable region of icicle ripples (case I), with contour lines displaying again ω_i and k_m. Since the value of the slope in this problem does not affect the results, this plot has been obtained by fixing $\beta = \pi/2$ and by varying the free surface temperature Θ_0^F in supercooled conditions. In the inset, the selected wavelength is also reported in millimeters versus the Reynolds number. We finally remind that, unlike the room air temperature (Θ_∞^a), the exact value of the temperature on the free surface (Θ_0^F) is usually unknown during the experiments. By analyzing the air boundary layer, it can be shown that $\Theta_0^F \sim r_{ka} D_a \Theta_\infty^a$, where r_{ka} is the ratio of thermal conductibility between the air and liquid and D_a is the dimensionless air boundary layer (see also Eq. (29) in Ref. [13]). Since $r_{ka} D_a \ll 1$, it follows that $|\Theta_0^F|$ can be also two orders of magnitude smaller than $|\Theta_\infty^a|$ (i.e., warmer than the surrounding air).

C. The cusp map method

In order to assess the nature of the instability, let us introduce the complex absolute wave number k_0 and the absolute growth rate $\omega_{0i} = \mathrm{Im}[\omega(k_0)]$. k_0 is the wave number that corresponds to the solution of the saddle point condition $\partial\omega/\partial k|_{k_0} = 0$, provided the causality principle is satisfied, i.e., (i) the complex $\{k_r, k_i\}$ plane displays the pinching point k_0 between two spatial branches $k^+(\omega_{0i})$ and $k^-(\omega_{0i})$ of the dispersion relation, and (ii) the spatial branches are well confined within their respective k_i half planes when $\omega_i \gg \omega_{0i}$. According to the Briggs criterion, the instability is convective if $\omega_i(k_m) > 0$ and $\omega_{0i} < 0$ and it is absolute if $\omega_r(k_m) > 0$ and $\omega_{0r} > 0$ [22,23].

The above criterion determines if the wave with zero group velocity is growing (absolute case) or decaying (convective case). This is an easy task only in a limited number of cases, where the dispersion relation is provided analytically and the value of k_0 can be obtained by solving a closed algebraic equation. This is not the case here since the solution of the eigenvalue problem [Eqs. (14)–(22)] is not given as an explicit dispersion relation. In order to circumvent this difficulty, we apply the so-called cusp map method [24], which requires only the mapping $k \to \omega$.

The cusp map method basically follows two steps. Firstly, wave numbers that give zero group velocity are identified. This is done by recalling that in the ω plane a point ω_0 satisfies the saddle point condition and displays a local map $(\omega - \omega_0) \sim (k - k_0)^2$. This implies that when a curve lying in the complex k plane and passing trough k_0 is mapped into the complex ω plane, it displays a cusplike singular point at the branch point ω_0. Kupfer et al. [24] suggested to map the contour $\mathrm{Im}[k] = k_i^*$, progressively altering k_i^* from zero in order to lower the mapping $k_i^* = 0$ towards $\omega_i = 0$. The mapping of all the contour points with $\mathrm{Im}[k] = k_i^*$ generates the curve $\Omega(k_i^*)$ in the complex frequency plane. A branch point is obtained when $\Omega(k_i^*)$ displays a cusplike singularity (occurring at ω_0). This occurs when $k_i^* = \mathrm{Im}(k_0)$.
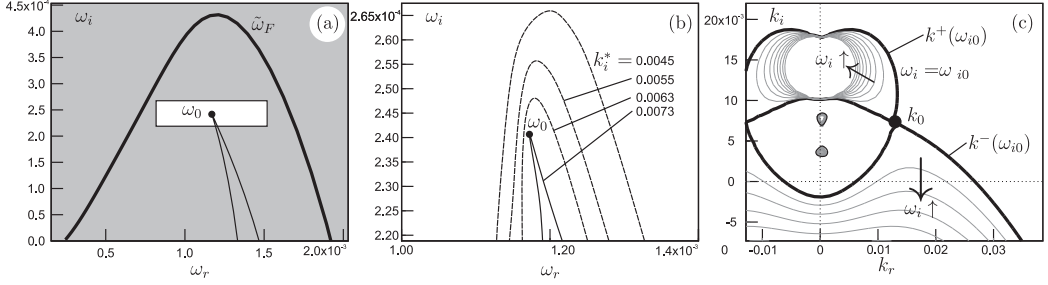
FIG. 5. (a) Cusp map in the ω plane for Re $= 800$, $\beta = 0.15$ rad, and $\Theta_0^F = 0.25$. The thick and thin lines are $\tilde{\omega}_F \equiv \Omega(0)$ and $\Omega(k_{0i})$, respectively. $\Omega(k_{0i})$ displays a branch point in ω_0. (b) Zoom-in of the white box surrounding the branching point. Thin solid line, $\Omega(k_{0i})$; dashed lines, selected mappings of $\Omega(k_i^*)$. (c) Behavior of the spatial branches in the k plane at the pinch point k_0 selected by the cusp map method. The arrows indicate in which direction the spatial branches move as ω_i attains large values.

Second, the check for the pinch point condition is performed by considering the relative position of ω_0 with respect to $\tilde{\omega}_F$, the latter being the mapping of $k_i^* = 0$ into the ω plane (i.e., the temporal branch). It can be demonstrated that branch points ω_0 that are "covered" an odd number of times by $\tilde{\omega}_F$ are pinch points [24] and therefore the causality principle is satisfied.

III. RESULTS

A first application of the cusp map method is reported in Figs. 5(a) and 5(b) for a particular case (Re $= 800, \beta = 0.15, \Theta_0^F = 0.25$). Since the imaginary part of the absolute growth rate ω_0 is positive, the instability is postulated to be absolute. This conjecture is definitively confirmed by observing that the curve $\tilde{\omega}_F$ covers only once the branch points ω_0 [bold curve in Fig. 5(a)], so it is an actual pinch point. In addition, a zoom-in, reported in Fig. 5(b), shows different mappings of the temporal branch curves for gradually increased values of k_i^*, which eventually generate a cusp at $k_i = k_{0i}$.

The same results can be obtained by the application of the Briggs criterion, as reported in Fig. 5(c). To this end, the eigenvalue problem was solved on a dense grid in the complex k plane, in a neighborhood of the absolute wave number $k_0 = \{k_{0r}, k_{0i}\}$, that was previously computed by the cusp method. The behavior of the spatial branches related to the pinch point $k_0 = 0.013 + 0.0073i$ is also shown. With the increase in ω_i (notice the trend indicated by the arrows), one of the two branches which merge at the pinch point is in the upper k_i half plane, while the other one is in the lower half plane. This ensures causality and confirms the absolute nature of the instability, as foreseen by the cusp map. It should be noticed that the plots reported in Fig. 5(c) have been facilitated by *a priori* knowledge of the location of the absolute wave number (via the cusp method). Otherwise its identification would have been so time demanding as to preclude an extensive exploitation of the Briggs criterion over the whole parameter space.

An extensive application of the cusp map method has been made first to the planar problem. A first result is that at inverted conditions ($\beta > \pi/2$) the instability is always convective, regardless the value of Re and β. On the other hand, when $\beta < \pi/2$, the instability can be both convective and absolute. The main outcome of the present work is reported in Fig. 6, where it is evident that with the increase in the Reynolds number, the system performs the standard stable–convectively unstable–absolutely unstable (S-CU-AU) scenario.

From the values reported by the contour lines of Fig. 6(a) the absolute character of the instability is particularly sharp at small slopes. Figure 6(b) instead reports the ratio between the real part of the absolute wave number and the most linearly unstable wave number. This ratio is almost everywhere smaller than unity, especially in the region where the instability is highly absolute. This implies that the wavelength of the wave with zero group velocity is larger than the most unstable wave. Since, in the laboratory frame, the absolute wavelength rules the asymptotic impulse response [17], this result
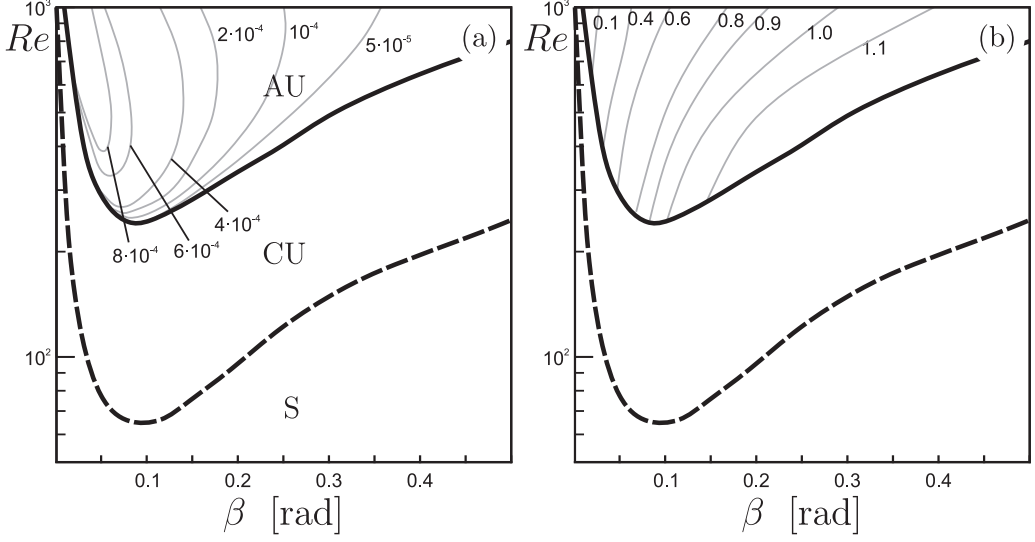
FIG. 6. (a) Absolute growth rate ω_{i0} in the $\{\beta, \text{Re}\}$ plane for $\Theta_0^F = 0.25$. The thick dashed line is the marginal stability curve (S is the stable zone). The thick continuous line separates the convective unstable (CU) zone from the absolutely unstable (AU) zone. (b) The ratio between the real part of the absolute wave number and the most linearly unstable wave number, i.e., $k_{r0}/k_{\max}$.

emphasizes that the long time behavior of the absolute instability is characterized by waves longer than those predicted by the classical linear instability.

A second important application of the method concerns the case of icicle ripples (Fig. 7). In this case, the domains of convective and absolute instability are located in a different way with respect
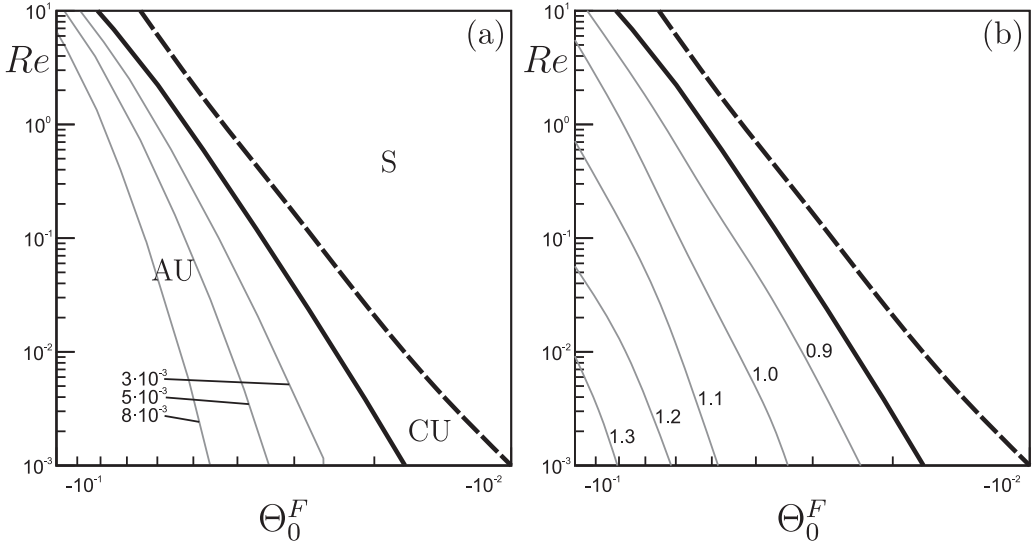

FIG. 7. (a) Absolute growth rate ω_{i0} in the $\{\Theta_0^F, \text{Re}\}$ plane for $\beta = \pi/2$. The thick dashed line is the marginal stability curve (S is the stable zone). The thick continuous line separates the convective unstable (CU) zone from the absolutely unstable (AU) zone. (b) The ratio between the real part of the absolute wave number and the most linearly unstable wave number, i.e., $k_{r0}/k_{\max}$.

to the planar case. In particular, if the surface temperature is kept fixed, with the increase in Re, the instability switches from absolute to convectively unstable. Finally, a further increment of Reynolds numbers stabilizes the system. The value of Re commonly used in the experiments is of the order of 10^{-1} or larger, while Θ_0^F is usually unknown, but on the basis of the reported room temperature ($-9\,°C$ in Ref. [13] and $-12\,°C$ in Ref. [15]) one can estimates that $|\Theta_0^F|$ is of order 10^{-2}. In these circumstances the system is stable or, at most, convectively unstable.

IV. DISCUSSION AND CONCLUSIONS

In the present work we have addressed the convective-absolute nature of the instability of a freezing-melting interface exposed to an open-channel flow. The issue has relevance in two typical phenomenological patterns: (i) ice ripples (and their evolution to cycle steps) which develop on gentle surfaces under relatively high Reynolds numbers and (ii) ripples which develop on icicles at small Reynolds numbers. Because of the mathematical complexity of the linearized problem, the use of the cusp map method has been necessary. Three important considerations arise.

First, the linear stability analysis carried out in the icicle regime selects a wavelength, provided the degree of supercooling is high enough and the Reynolds number is small. With the increase in Re, a transition from absolutely unstable to convectively unstable and eventually to stable is observed. We notice that common experimental setups are usually away from the domain of existence of icicle ripples here obtained. Furthermore, the wavelength selected is on the order of millimeters, which in a laboratory context can be read as noise. These outcomes are in line with the observations made by Chen and Morris [15], where icicles exposed to dripping water and in the absence of dissolved salt did not develop a visible pattern formation (whereas when NaCl was dissolved, centimetric patterns occurred). Incidentally, it should also be noticed that, since Re increases with a decrease in the icicle radius, downstream migration of the wavelet corresponds to an upward movement in Fig. 3(a) and a growth rate becoming smaller and smaller. It was already conjectured that the observations reported in Ref. [15] could be explained in terms of icicle-fluting transition (namely a violation of Squire's theorem) occurring at very small values of Re, such as those reported in the experiments [21].

Second, the contour lines reported in Fig. 6(b) suggest that the asymptotic behavior of the absolutely unstable patterns in the planar case usually exhibit longer waves than the most unstable ones. This result is in agreement with the recent observations in Ref. [9], where laboratory experiments showed that the asymptotic wavelengths are longer than those theoretically predicted by the linearized problem. The authors attributed this fact to the nonlinear evolution to cycle steps, but the absolute character of the instability could also play a role in this discrepancy.

Third, if Fig. 6 is crossed with a horizontal line, where Re $\geqslant 200$ is kept constant and the slope is gradually increased, the typical CU-AU-CU scenario occurs, which is commonplace in hydrodynamics (e.g., the wake behind a bluff body). Increasing the slope conceptually corresponds to moving downstream over a convex ice-water interface in which the liquid flow rate per unit width, q, remains constant, the slope and velocity increase, and the depth decreases, but Re $= q/\nu$ does not change. This condition is typical of melting supraglacial water flowing over glacier snouts (the lowest end of a mountain glacier), where nonparallel effects related to the decrease of the depth at the base state can become important and the stability analysis must be considered from a *global* point of view [17] (here we just focused on a *local* analysis). If the degree of nonparallelism is small (namely the glacier convexity is small), the problem can be tackled by multiple scaling and becomes formally equivalent to the study of spatially developing flows encountered in open shear flow instabilities described in Ref. [25]. This task is far from the aim of the present paper but it proposes possible future developments. Other unsolved issues that would deserve further attention concern the nonlinear evolution of these patterns and the role of temporal variability of the flow rate in pattern formation.

[1] K. Pye and H. Tsoar, *Aeolian Sand and Sand Dunes* (Unwin Hyman, London, 1990).

[2] M. Frezzotti, S. Gandolfi, and S. Urbini, Snow megadunes in Antarctica: Sedimentary structure and genesis, J. Geophys. Res. Atmos. **107**, 4344 (2002).

[3] D. Knighton, *Fluvial Forms and Processes: A New Perspective* (Arnold, London, 1998).

[4] I. J. Fairchild, C. L. Smith, A. Baker, L. Fuller, C. Spötl, D. Mattey, F. McDermott, and Edinburgh Ion Microprobe Facility, Modification and preservation of environmental signals in speleothems, Earth Sci. Rev. **75**, 105 (2006).

[5] L. Solari and G. Parker, Morphodynamic modeling of the basal boundary of ice cover on brackish lakes, J. Geophys. Res. Earth Surf. **118**, 1432 (2013).

[6] A. Fowler, *Mathematical Geosciences* (Springer, Berlin, 2011).

[7] See http://www.nimbus.it/ghiacciai/2006/060915ciardoney.htm for other data and pictures.

[8] C. Camporeale and R. Ridolfi, Hydrodynamic-Driven Stability Analysis of Morphological Patterns on Stalactites and Implications for Cave Paleoflow Reconstructions, Phys. Rev. Lett. **108**, 238501 (2012).

[9] M. Yokokawa, N. Izumi, K. Naito, G. Parker, T. Yamada, and R. Greve, Cyclic steps on ice, J. Geophys. Res. Earth Surf. **121**, 1023 (2016).

[10] G. D. Ashton and J. F. Kennedy, Ripples on underside of river ice covers, J. Hydraul. Div. ASCE **100**, 479 (1974).

[11] R. R. Gilpin, Ice formation in a pipe containing flows in the transition and turbulent regimes, J. Heat Transfer **103**, 363 (1981).

[12] K. Ueno, Pattern formation in crystal growth under parabolic shear flow, Phys. Rev. E **68**, 021603 (2003).

[13] K. Ueno, M. Farzaneh, S. Yamaguchi, and H. Tsuji, Numerical and experimental verification of a theoretical model of ripple formation in ice growth under supercooled water film flow, Fluid Dyn. Res. **42**, 025508 (2010).

[14] C. Camporeale and L. Ridolfi, Ice ripple formation at large Reynolds numbers, J. Fluid Mech. **694**, 225 (2012).

[15] A. S.-H. Chen and S. W. Morris, On the origin and evolution of icicle ripples, New J. Phys. **15**, 103012 (2013).

[16] P. J. Schmid and D. S. Henningson, *Stability and Transition in Shear Flows*, 1st ed. (Springer, Berlin, 2001).

[17] P. Huerre and M. Rossi, Hydrodynamic instabilities in open flows, in *Hydrodynamic and Nonlinear Instabilities*, edited by C. Goldreche and P. Manneville (Cambridge University Press, Cambridge, UK, 2000), pp. 159–229.

[18] R. Vesipa, C. Camporeale, L. Ridolfi, and J. M. Chomaz, On the convective-absolute nature of river bedform instabilities, Phys. Fluids **26**, 124104 (2014).

[19] A. S.-H. Chen, Experiments on the growth and form of icicles, Ph.D. thesis, University of Toronto, 2014.

[20] R. Vesipa, C. Camporeale, and L. Ridolfi, Thin-film-induced morphological instabilities over calcite surfaces, Proc. R. Soc. A **471**, 20150031 (2015).

[21] C. Camporeale, Hydrodynamically locked morphogenesis in karst and ice flutings, J. Fluid Mech. **778**, 89 (2015).

[22] R. J. Briggs, *Electron-Stream Interaction with Plasma* (MIT Press, Boston, 1964).

[23] A. Bers, Space-time evolution of plasma instabilities—absolute and convective, in *Handbook of Plasma Physics*, edited by M. Rosenbluth and R. Sagdeev (North Holland, Amsterdam, 1983), pp. 159–229.

[24] K. Kupfer, A. Bers, and A. K. Ram, The cusp map in the complex-frequency plane for absolute instabilities, Phys. Fluids **30**, 3075 (1987).

[25] P. Huerre and P. A. Monkewitz, Local and global instabilities in spatially developing flows, Annu. Rev. Fluid Mech. **22**, 473 (1990).